Editors' Suggestion | Featured in Physics

Experimental Property Reconstruction in a Photonic Quantum Extreme Learning Machine

Alessia Suprano,[1,*] Danilo Zia,[1,*] Luca Innocenti,[2,*] Salvatore Lorenzo,[2,*] Valeria Cimini,[1] Taira Giordani,[1] Ivan Palmisano,[3] Emanuele Polino,[1,4] Nicolò Spagnolo,[1] Fabio Sciarrino,[1,†] G. Massimo Palma,[2] Alessandro Ferraro,[3,5] and Mauro Paternostro[2,3,‡]

[1]*Dipartimento di Fisica - Sapienza Università di Roma, Piazza le Aldo Moro 5, I-00185 Roma, Italy*
[2]*Università degli Studi di Palermo, Dipartimento di Fisica e Chimica - Emilio Segrè, via Archirafi 36, I-90123 Palermo, Italy*
[3]*Centre for Quantum Materials and Technologies, School of Mathematics and Physics, Queen's University Belfast, BT7 1NN, United Kingdom*
[4]*Centre for Quantum Dynamics and Centre for Quantum Computation and Communication Technology, Griffith University, Yuggera Country, Brisbane, Queensland 4111, Australia*
[5]*Quantum Technology Lab, Dipartimento di Fisica Aldo Pontremoli, Università degli Studi di Milano, I-20133 Milano, Italy*

(Received 14 November 2023; accepted 7 March 2024; published 16 April 2024)

Recent developments have led to the possibility of embedding machine learning tools into experimental platforms to address key problems, including the characterization of the properties of quantum states. Leveraging on this, we implement a quantum extreme learning machine in a photonic platform to achieve resource-efficient and accurate characterization of the polarization state of a photon. The underlying reservoir dynamics through which such input state evolves is implemented using the coined quantum walk of high-dimensional photonic orbital angular momentum and performing projective measurements over a fixed basis. We demonstrate how the reconstruction of an unknown polarization state does not need a careful characterization of the measurement apparatus and is robust to experimental imperfections, thus representing a promising route for resource-economic state characterization.

DOI: 10.1103/PhysRevLett.132.160802

Context and motivations.—Accurate and resource-efficient estimation of properties of quantum states is a pivotal task in quantum information science, particularly in areas such as quantum metrology [1–4]. In particular, estimation strategies relying on single measurement settings have attracted notable attention in the past years [5–8]. Significant attention has also been devoted to the theoretical analysis of state estimation protocols based on randomized measurements, in particular, through shadow tomography protocols [5,9–12], which were later shown to be applicable in generic measurement scenarios [13–15]. On the other hand, several works have demonstrated the usefulness of integrating machine learning tools to implement and enhance the efficiency of quantum state estimation strategies [16–28]. In particular, quantum extreme learning machines (QELMs) [29,30] have been proposed as a particularly efficient medium to extract features from input quantum states with a flexible architecture [14,31,32].

In this Letter, we leverage QELMs to efficiently recover properties of photonic quantum states encoded in the polarization degree of freedom, exploiting orbital angular momentum (OAM) as an ancillary degree of freedom to enable reconstruction via a single measurement setting. The interaction between polarization and OAM, which is experimentally implemented via a quantum-walk-based photonic apparatus [33,34], allows to extract information about the input polarization state by measuring only the OAM of the final state. In the context of QELMs, the evolution mapping input polarization to output OAM takes the role of "reservoir dynamics" and enables complete reconstruction using a single measurement basis. Using the framework of QELMs has the significant advantage of enabling the retrieval of information about the input state even without complete knowledge of the experimental apparatus itself. This makes for an extremely flexible platform to extract features of input states and is in stark contrast with conventional reconstruction pipelines, which crucially rely on accurate models of the evolution and measurement undergone by the states. QELMs operate effectively without this assumption, requiring only access to a training dataset of known states—a task that is often less demanding in practice. While experimental demonstrations of single-setting quantum state estimation have been reported in a few different platforms [5–7], reconstructions in all such protocols rely on accurate prior knowledge of all parts of the experimental apparatus. By contrast, our QELM-based strategy makes for a highly flexible estimation strategy, resilient to many types of

experimental noise and misalignment, by virtue of the training stage automatically adapting the postprocessing to enable accurate reconstruction. We benchmark our results with the accuracies obtained using alternative estimation strategies, finding our QELM-based approach to clearly outperform the alternatives in the considered scenarios. It is worth noting that the reported reconstruction strategy is fully general and applicable to any experimental scenario where the goal is reconstructing properties of input states, even though only a partially characterized measurement stage is available. Furthermore, as discussed in depth in Refs. [14,35], the statistics required for accurate reconstruction mostly depend on the symmetry properties of the effective measurement implemented by the setup rather than the dimension of the state one wishes to reconstruct.

QELM estimation framework.—QELMs operate by exploiting an uncharacterized time-independent dynamics to extract target properties from input states. To achieve this, the scheme uses a training dataset of quantum states to figure out the best way to extract the sought-after features from the measurement data [14]. The use of a training dataset allows one to forgo the need to characterize the measurement apparatus itself: The training process automatically adjusts to the complexities of the experimental reality. Furthermore, training QELMs is a particularly simple endeavor, amounting to solving a linear regression problem, and is, therefore, less prone to overfitting issues, especially when used to extract linear features such as expectation values of observables [14]. More formally, a QELM involves evolving input states ρ through some quantum channel Φ—giving rise to what we will refer to as *reservoir dynamics* hereafter—and then measuring them with some positive operator-valued measure (POVM) $\boldsymbol{\mu} \equiv (\mu_b)_b$. Using a training dataset of the form $\{(\boldsymbol{p}_k^{\mathrm{tr}}, o_k)\}_k$ with $\boldsymbol{p}_k^{\mathrm{tr}}$ the probability vector resulting from measuring ρ_k^{tr}, $(\boldsymbol{p}_k^{\mathrm{tr}})_b \equiv \mathrm{tr}(\mu_b \rho_k^{\mathrm{tr}})$, and $o_k \equiv \mathrm{tr}(\mathcal{O}\rho_k^{\mathrm{tr}})$ for some target observable $\mathcal{O}$, one can find a linear transformation $\boldsymbol{w} \equiv (w_b)_b$ such that $\sum_b w_b \mathrm{tr}(\mu_b \rho) \approx \mathrm{tr}(\mathcal{O}\rho)$ for all ρ. In words, finding this $\boldsymbol{w}$ allows to read the target expectation values of input states directly from the measurement data, without requiring knowledge on the dynamics Φ and on the POVM $\boldsymbol{\mu}$ themselves (see Supplemental Material for more details [36]). This protocol can be seamlessly adapted to the case of multiple target observables. The expressivity of a QELM—that is, the space of observables that can be accurately retrieved for a given choice of Φ and $\boldsymbol{\mu}$—was proven to depend exclusively on the properties of the "effective POVM," that is, the POVM with elements $\tilde{\mu}_b \equiv \Phi^\dagger(\mu_b)$, where $\Phi^\dagger$ denotes the adjoint of Φ [41]. In particular, a necessary condition for enabling the reconstruction of arbitrary observables is that the reservoir dynamics Φ must enlarge the dimension of the input space in order to guarantee a sufficiently large number of measurement outcomes [14].

Experimental estimation strategy.—We implement experimentally the QELM-based quantum state estimation strategy using as reservoir dynamics a coined quantum walk (QW) in polarization and OAM of single photons [33,34]. The goal of the protocol is to extract expectation values of observables on the input polarization states, using the reservoir dynamics to transfer this information into the larger OAM space that is then measured [see Fig. 1(a)]. More specifically, we use states of the form $|\Psi_f\rangle = (\prod_{k=1}^{s} SC_k)|0,\psi\rangle$, with $C_k \equiv I \otimes U_k$ the unitary *coin operation*, acting nontrivially only on the coin space,

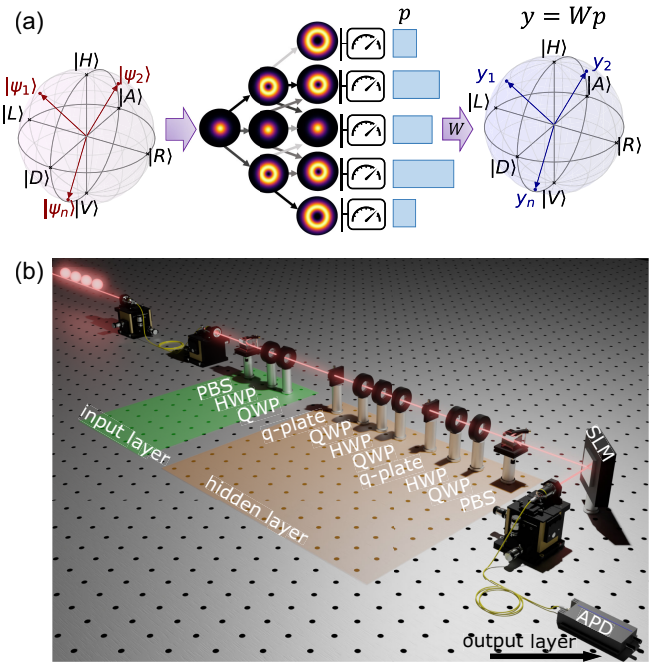

FIG. 1. Experimental QELM. (a) Schematic overview of the experimental QELM. Initial quantum states $|\psi_1\rangle, |\psi_2\rangle, \ldots, |\psi_n\rangle$ encoded in the polarization degree of freedom of single photons evolve through a reservoir dynamics, in which the information encoded in the initial two-dimensional space is transferred into the larger Hilbert space of the OAM. By performing only projective measurements on the OAM computational basis, the QELM is trained to reconstruct a set of target values $y_1, y_2, \ldots, y_n$. (b) Experimental implementation. Single photons, generated at 808 nm via spontaneous parametric down-conversion, are sent through the state-preparation stage (*input layer*) made by a polarizing-beam splitter (PBS), a half-wave plate (HWP), and a quarter-wave plate (QWP) to encode the initial state in the polarization degree of freedom. Subsequently, the input states evolve through the *hidden layer* following the quantum walk dynamics implemented by HWPs, QWPs, and q plates (QPs). After projecting onto the polarization state $|\psi_{\mathrm{pol}}\rangle$ with a sequence of HWP, QWP, and PBS, projective measurements in the OAM computational basis, $\mathcal{B} = \{|n\rangle\}$ with $n = \{-2, \ldots, 2\}$, are performed through a spatial light modulator (SLM) followed by the coupling into a single-mode fiber. From the counts measured by an avalanche photodiode (APD), the output layer of the QELM is trained to retrieve the expectation values of the observables $\{\sigma_x, \sigma_y, \sigma_z\}$.

and with $S \equiv \sqrt{p}(I \otimes |\downarrow\rangle\langle\downarrow| + I \otimes |\uparrow\rangle\langle\uparrow|) + \sqrt{1-p}(E_- \otimes |\downarrow\rangle\langle\uparrow| + E_+ \otimes |\uparrow\rangle\langle\downarrow|)$ a *partial* controlled-shift operation, which differs from the standard control-shift gate by also allowing the walker state to not change with some probability. Here, $\{|\uparrow\rangle, |\downarrow\rangle\}$ is the computational basis for the coin space, I is the identity operator on the walker space, $E_\pm|j\rangle \equiv |j \pm 1\rangle$, with $\{|j\rangle\}$, $j = -N, \ldots, N$ the position states of the walker, living in a $(2N+1)$-dimensional Hilbert space, and $E_-|-N\rangle = E_+|N\rangle = 0$. Finally, $|\psi\rangle$ is the input polarization state we seek to characterize.

After the QW evolution, the polarization is projected on some state $|\psi_{\text{pol}}\rangle$, and the OAM is measured in its computational basis. To connect this with the general formalism introduced above, denote with U the unitary corresponding to the quantum walk dynamics, $|0_{\text{OAM}}\rangle$ the initial reference OAM state. The map describing the reservoir is $\Phi(\rho) = A\rho A^\dagger$, where $A \equiv (\langle\psi_{\text{pol}}| \otimes I_{\text{OAM}})\, U(I_{\text{pol}} \otimes |0_{\text{OAM}}\rangle)$. The final measurement on the OAM is then a standard projective measurement in the computational basis $\mu_b = |b\rangle\langle b|$, with a number of outcomes that depends on the number of QW steps.

Optical setup.—In the experimental setup, reported in Fig. 1(b), a set of optical elements composed of a polarizing beam splitter, a half-wave plate [HWP (ζ_1)], and a quarter-wave plate [QWP (θ_1)] produces an input polarization state parametrized as

$$|\psi\rangle = \frac{1}{\sqrt{2}}\{e^{i\theta_1}[\cos(2\zeta_1 - \theta_1) - \sin(2\zeta_1 - \theta_1)]|L\rangle + e^{-i\theta_1}[\cos(2\zeta_1 - \theta_1) + \sin(2\zeta_1 - \theta_1)]|R\rangle\}, \quad (1)$$

where $|L\rangle$ and $|R\rangle$ stand for left- and right-circular polarization, respectively, and θ_1 and ζ_1 are the rotation angles of the wave plate optical axis. The input state then evolves through a series of half-wave plates [HWP (ζ)], quarter-wave plates [QWP (θ))], and an inhomogeneous birefringent device, known as q plate [QP (α, δ)], which couples polarization and OAM conditionally on the parameters δ, the tunable phase retardance that allows the optimal tuning of the device when $\delta = \pi$, and α, which is a characteristic angle associated to the initial orientation of the optical axis with respect to the horizontal direction. QPs have been used as a building block in a significant number of demonstrations of controlled quantum dynamics [42,43] and are, in particular, often used as controlled-shift gate to implement QW dynamics [17,34,44–48]. The coin operation is implemented via a sequence of wave plates as $C(\zeta, \theta, \phi) = \text{QWP}(\zeta)\text{HWP}(\theta)\text{QWP}(\phi)$, with ζ, θ, ϕ tunable angles. Each q plate implements a controlled-shift operation $S(\alpha, \delta)$ with characteristic parameters α and δ. More explicitly, these operations take the form

$$C(\zeta, \theta, \phi) = \begin{pmatrix} e^{-i(\zeta-\phi)}\cos\eta & e^{i(\zeta+\phi)}\sin\eta \\ -e^{-i(\zeta+\phi)}\sin\eta & e^{i(\zeta-\phi)}\cos\eta \end{pmatrix}, \quad (2)$$

$$S(\alpha, \delta) = \sum_{n=-N+1}^{N-1} \cos\frac{\delta}{2}(|L, n\rangle\langle L, n| + |R, n\rangle\langle R, n|) + i\sin\frac{\delta}{2}(e^{2i\alpha}|L, n\rangle\langle R, n+1| + e^{-2i\alpha}|R, n\rangle \times \langle L, n-1|), \quad (3)$$

with $\eta = \zeta + \phi - 2\theta$.

Here, $|L, n\rangle$ ($|R, n\rangle$) denote left- (right-) circular polarization, and OAM with azimuthal quantum number n. The overall evolution U implemented by our apparatus is obtained by combining two controlled-shift and one coin operation:

$$U = S(\alpha_2, \pi)C(\zeta, \theta, \phi)S(\alpha_1, \pi/2), \quad (4)$$

where α_1 and α_2 are fixed by the fabrication process and in our case equal 105° and 336°, respectively. Another coin operation is used at the beginning to prepare the input state [see Eq. (1)] and is, thus, not considered as part of the reservoir dynamics. Fixing the parameters δ of the q plates to π and $\pi/2$, respectively, allows us to enlarge the space of reachable output OAM states without adding QW steps, thanks to the stationary component of the dynamics. After evolution through U, a combination of wave plates and a polarizing beam splitter are used to project the polarization, while a spatial light modulator (SLM) and a single-mode fiber are employed to measure the final OAM states, obtaining the occupation probabilities for the basis states $|n\rangle$, $n = -2, -1, 0, 1, 2$. The single-photon counts are then collected and fed to the computer, where postprocessing and training of the QELM take place, and the target expectation values are estimated.

Results.—We considered two different configurations for the QELM. In the first, we exploited the knowledge of the QW dynamics to extract optimal values for the angles of the coin $\{\zeta, \theta, \phi\}$ and for the projection of the hidden layer which result in an almost uniform cover of the OAM space (see Supplemental Material [36]). In the second one, instead, we made a random choice of the wave plate angles, focusing on training the accessible output layer to optimize the performance of the characterization protocol. The chosen figure of merit for the quantification of performances is the mean square error (MSE) between the expectation values of the Pauli operators. The experimental results are reported in Fig. 2 for both implementations. We show the performance of QELM, trained using experimental data, in retrieving the features of the polarization state. In particular, we collected 300 experimental states and split them into a training set and a test set, each one composed of 150 elements. The MSE of the expectation values over the test set is studied against the number N_{train} of states used in the training set. A large enough training set clearly results in a decrease of the MSE and, thus, in significantly enhanced reconstruction accuracies for all

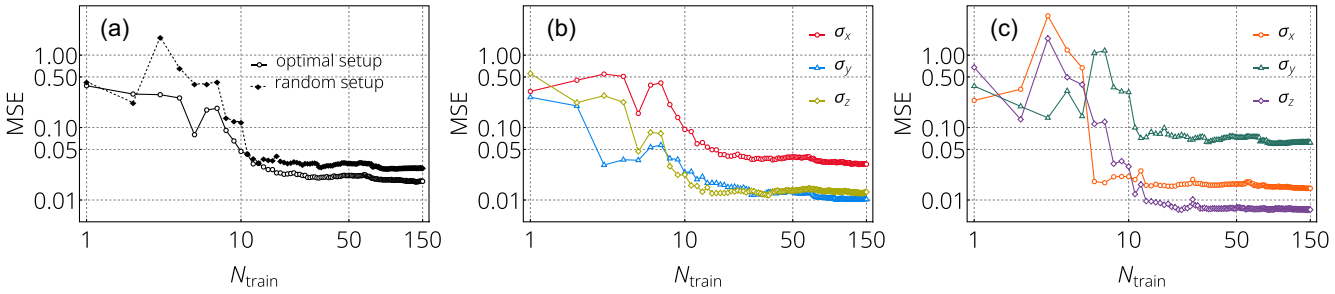

FIG. 2. Experimental results. Estimation MSE obtained by training and testing the QELM with experimental data. The target is estimating the expectation values of the Pauli matrices σ_x, σ_y, σ_z on the input polarization state. We study the MSE as a function of the number of training states N_{train}, at fixed statistics N. To test the protocol, we generated 300 random input states and tested the estimation when the first $1 \leq N_{\text{train}} \leq 150$ are used to train the QELM. The set of 300 states remains unchanged throughout all experiments. The last 150 of these 300 states are always used for testing, to compute the MSE. All the points in the saturated regions of these figures decrease as $1/N$ when increasing the statistics with which each training and test state is measured. (a) Average of the MSE estimated for all three target observables: $\{\sigma_x, \sigma_y, \sigma_z\}$. We show the results for both optimized and random setups. (b) MSE for each individual target observable for the optimized setup. (c) MSE for each individual target observable for the random setup. The reported results are obtained with average experimental statistics of ∼3000 counts.

considered target observables. The amount of statistics collected for each state also crucially affects the reconstruction accuracies [14]. We analyze this aspect explicitly in Supplemental Material [36].

Let us remark here other two significant aspects that transpire from our experimental results. First, our reconstruction protocol is highly resource efficient; indeed, roughly 20 states are already sufficient to train the QELM, as seen in Fig. 2. Second, as shown in Fig. 2(a), the optimal configuration results in MSEs only marginally better than those obtained with the random configuration, highlighting that a full characterization and fine-tuning of the experimental setup is not essential to achieve accurate reconstruction accuracies (see details in Supplemental Material [36]).

Finally, to compare the quality of the results obtained via the QELM with non-machine-learning-based alternative approaches, we consider the reconstruction MSEs that would have been obtained with the same experimental apparatus via the generalized shadow tomography reconstruction scheme, which has been shown to be optimal for reconstruction under relatively mild assumptions [35]. As discussed in detail in Supplemental Material [36], we find that the QELM provides performances between 5 and 10 times better than the alternative methods for the considered target observables, in the case of the optimal experimental setup. A main underlying reason for this disparity is that the non-QELM-based methods rely on accurate modeling of the experimental apparatus, which can be quite costly to achieve in practice, whereas QELM can easily adapt to experimental fluctuations without significantly impacting the reconstruction accuracies.

Conclusions.—We have experimentally demonstrated a robust and resource-efficient QELM-based property reconstruction protocol. Our implementation, which leverages the controlled QW dynamics in a photonic platform intertwining the polarization and OAM degrees of freedom of a photon, demonstrates the excellent performance of property reconstruction without the need for the accurate and careful characterization of the platform. Only training sets with moderate size are needed to achieve low values of the MSE of the reconstruction, while the effects of finite statistics of the dataset can be fully accounted for. Our experimental QELM-based reconstruction demonstrates the viability of photonic platforms for nonstandard approaches to quantum property retrieval, with the expectation of significantly reducing the burden—in terms of resources—of resource characterization in a computational register.

A. F., S. L., and G. M. P. acknowledge support by MUR under PRIN Project No. 2022FEXLYB Quantum Reservoir Computing (QuReCo). L. I. acknowledges support from MUR and AWS under project PON Ricerca e Innovazione 2014-2020, "Calcolo quantistico in dispositivi quantistici rumorosi nel regime di scala intermedia" (NISQ—Noisy, Intermediate-Scale Quantum). I. P. is grateful to the MSCA COFUND project Collaboration in Training and Innovation for Growing, Evolving and Networked Societies (Grant No. 945231). M. P. acknowledges the support by the European Union's Horizon 2020 FET-Open project Testing the Large-Scale Limit of Quantum Mechanics (Grant Agreement No. 766900), the Horizon Europe EIC Pathfinder project Quantum Control of Gravity with Levitated Mechanics (Grant Agreement No. 101046973), the Leverhulme Trust Research Project Grant UltraQuTe (Grant No. RPG-2018-266), the Royal Society Wolfson Fellowship (RSWF/R3/183013), the United Kingdom EPSRC (EP/T028424/1), and the Department for the Economy Northern Ireland under the U.S.–Ireland R&D Partnership Program (USI 175 and USI 194). A. S., V. C., T. G., E. P., D. Z., N. S., F. S. acknowledges support from

the ERC Advanced Grant QU-BOSS (QUantum advantage via nonlinear BOSon Sampling, Grant Agreement No. 884676) and from PNRR MUR Project No. PE0000023-NQSTI (Spoke 4).

*These authors contributed equally to this work.
†Corresponding author: fabio.sciarrino@uniroma1
‡Corresponding author: mauro.paternostro@unipa.it

[1] E. Polino, M. Valeri, N. Spagnolo, and F. Sciarrino, Photonic quantum metrology, AVS Quantum Sci. **2**, 024703 (2020).
[2] V. Giovannetti, S. Lloyd, and L. Maccone, Advances in quantum metrology, Nat. Photonics **5**, 222 (2011).
[3] A. Czerwinski, Selected concepts of quantum state tomography, Optics **3**, 268 (2022).
[4] V. Gebhart, R. Santagati, A. A. Gentile, E. M. Gauger, D. Craig, N. Ares, L. Banchi, F. Marquardt, L. Pezzè, and C. Bonato, Learning quantum systems, Nat. Rev. Phys. **5**, 141 (2023).
[5] R. Stricker, M. Meth, L. Postler, C. Edmunds, C. Ferrie, R. Blatt, P. Schindler, T. Monz, R. Kueng, and M. Ringbauer, Experimental single-setting quantum state tomography, PRX Quantum **3**, 040310 (2022).
[6] Z. Bian, J. Li, H. Qin, X. Zhan, R. Zhang, B. C. Sanders, and P. Xue, Realization of single-qubit positive-operator-valued measurement via a one-dimensional photonic quantum walk, Phys. Rev. Lett. **114**, 203602 (2015).
[7] C. A. Galvis-Florez, D. Reitzner, and S. Särkkä, Single qubit state estimation on NISQ devices with limited resources and sic-povms, arXiv:2308.07664.
[8] G. I. Struchalin, Y. A. Zagorovskii, E. V. Kovlakov, S. S. Straupe, and S. P. Kulik, Experimental estimation of quantum state properties from classical shadows, PRX Quantum **2**, 010307 (2021).
[9] H.-Y. Huang, R. Kueng, and J. Preskill, Predicting many properties of a quantum system from very few measurements, Nat. Phys. **16**, 1050 (2020).
[10] Y. Zhou and Q. Liu, Performance analysis of multi-shot shadow estimation, Quantum **7**, 1044 (2023).
[11] A. Elben, S. T. Flammia, H.-Y. Huang, R. Kueng, J. Preskill, B. Vermersch, and P. Zoller, The randomized measurement toolbox, Nat. Rev. Phys. **5**, 9 (2023).
[12] M. C. Tran, D. K. Mark, W. W. Ho, and S. Choi, Measuring arbitrary physical properties in analog quantum simulation, Phys. Rev. X **13**, 011049 (2023).
[13] A. Acharya, D. Banerjee, and S. Bhattacharya, Shadow tomography based on informationally complete positive operator-valued measure, Phys. Rev. A **104**, 052418 (2021).
[14] L. Innocenti, S. Lorenzo, I. Palmisano, A. Ferraro, M. Paternostro, and G. M. Palma, On the potential and limitations of quantum extreme learning machines, Commun. Phys. **6**, 118 (2023).
[15] H. C. Nguyen, J. L. Bönsel, J. Steinberg, and O. Gühne, Optimising shadow tomography with generalised measurements, Phys. Rev. Lett. **129**, 220502 (2022).
[16] T. Giordani, A. Suprano, E. Polino, F. Acanfora, L. Innocenti, A. Ferraro, M. Paternostro, N. Spagnolo, and F. Sciarrino, Machine learning-based classification of vector vortex beams, Phys. Rev. Lett. **124**, 160401 (2020).
[17] A. Suprano, D. Zia, E. Polino, T. Giordani, L. Innocenti, A. Ferraro, M. Paternostro, N. Spagnolo, and F. Sciarrino, Dynamical learning of a photonics quantum-state engineering process, Adv. Photonics **3**, 066002 (2021).
[18] A. Suprano, D. Zia, E. Polino, T. Giordani, L. Innocenti, M. Paternostro, A. Ferraro, N. Spagnolo, and F. Sciarrino, Enhanced detection techniques of orbital angular momentum states in the classical and quantum regimes, New J. Phys. **23**, 073014 (2021).
[19] D. Zia, R. Checchinato, A. Suprano, T. Giordani, E. Polino, L. Innocenti, A. Ferraro, M. Paternostro, N. Spagnolo, and F. Sciarrino, Regression of high-dimensional angular momentum states of light, Phys. Rev. Res. **5**, 013142 (2023).
[20] S. Lohani, B. T. Kirby, M. Brodsky, O. Danaci, and R. T. Glasser, Machine learning assisted quantum state estimation, Mach. Learn. **1**, 035007 (2020).
[21] A. Melnikov, M. Kordzanganeh, A. Alodjants, and R.-K. Lee, Quantum machine learning: From physics to software engineering, Adv. Phys. **8**, 2165452 (2023).
[22] A. Rocchetto, S. Aaronson, S. Severini, G. Carvacho, D. Poderini, I. Agresti, M. Bentivegna, and F. Sciarrino, Experimental learning of quantum states, Sci. Adv. **5**, eaau1946 (2019).
[23] R. Santagati, J. Wang, A. A. Gentile, S. Paesani, N. Wiebe, J. R. McClean, S. Morley-Short, P. J. Shadbolt, D. Bonneau, J. W. Silverstone, D. P. Tew, X. Zhou, J. L. O'Brien, and M. G. Thompson, Witnessing eigenstates for quantum simulation of Hamiltonian spectra, Sci. Adv. **4**, aap9646 (2018).
[24] J. Wang, S. Paesani, R. Santagati, S. Knauer, A. A. Gentile, N. Wiebe, M. Petruzzella, J. L. O'Brien, J. G. Rarity, A. Laing *et al.*, Experimental quantum Hamiltonian learning, Nat. Phys. **13**, 551 (2017).
[25] J. Carrasquilla, G. Torlai, R. G. Melko, and L. Aolita, Reconstructing quantum states with generative models, Nat. Mach. Intell. **1**, 155 (2019).
[26] V. Cimini, M. Valeri, E. Polino, S. Piacentini, F. Ceccarelli, G. Corrielli, N. Spagnolo, R. Osellame, and F. Sciarrino, Deep reinforcement learning for quantum multiparameter estimation, Adv. Photonics **5**, 016005 (2023).
[27] A. M. Palmieri, E. Kovlakov, F. Bianchi, D. Yudin, S. Straupe, J. D. Biamonte, and S. Kulik, Experimental neural network enhanced quantum tomography, npj Quantum Inf. **6**, 1 (2020).
[28] S. Ahmed, C. Sanchez Muñoz, F. Nori, and A. F. Kockum, Quantum state tomography with conditional generative adversarial networks, Phys. Rev. Lett. **127**, 140502 (2021).
[29] P. Mujal, R. Martínez-Peña, J. Nokkala, J. García-Beni, G. L. Giorgi, M. C. Soriano, and R. Zambrini, Opportunities in quantum reservoir computing and extreme learning machines, Adv. Quantum Technol. **4**, 2100027 (2021).
[30] G.-B. Huang, D. H. Wang, and Y. Lan, Extreme learning machines: A survey, Int. J. Mach. Learn. Cybern. **2**, 107 (2011).
[31] S. Ghosh, A. Opala, M. Matuszewski, T. Paterek, and T. C. Liew, Quantum reservoir processing, npj Quantum Inf. **5**, 35 (2019).

[32] T. Krisnanda, H. Xu, S. Ghosh, and T. C. H. Liew, Tomographic completeness and robustness of quantum reservoir networks, Phys. Rev. A **107**, 042402 (2023).
[33] L. Innocenti, H. Majury, T. Giordani, N. Spagnolo, F. Sciarrino, M. Paternostro, and A. Ferraro, Quantum state engineering using one-dimensional discrete-time quantum walks, Phys. Rev. A **96**, 062326 (2017).
[34] T. Giordani, E. Polino, S. Emiliani, A. Suprano, L. Innocenti, H. Majury, L. Marrucci, M. Paternostro, A. Ferraro, N. Spagnolo *et al.*, Experimental engineering of arbitrary qudit states with discrete-time quantum walks, Phys. Rev. Lett. **122**, 020503 (2019).
[35] L. Innocenti, S. Lorenzo, I. Palmisano, F. Albarelli, A. Ferraro, M. Paternostro, and G. M. Palma, Shadow tomography on general measurement frames, PRX Quantum **4**, 040328 (2023).
[36] See Supplemental Material at http://link.aps.org/supplemental/10.1103/PhysRevLett.132.160802, which includes Refs. [14,35,37–40], for further details on the theoretical background and on the effect of experimental imperfections.
[37] A. J. Scott, Tight informationally complete quantum measurements, J. Phys. A **39**, 13507 (2006).
[38] H. Zhu and B.-G. Englert, Quantum state tomography with fully symmetric measurements and product measurements, Phys. Rev. A **84**, 022327 (2011).
[39] J. Haah, A. W. Harrow, Z. Ji, X. Wu, and N. Yu, Sample-optimal tomography of quantum states, in *Proceedings of the Forty-Eighth Annual ACM Symposium on Theory of Computing* (Association for Computing Machinery, New York, 2016), pp. 913–925.
[40] A. Bisio, G. Chiribella, G. M. D'Ariano, S. Facchini, and P. Perinotti, Optimal quantum tomography, IEEE J. Sel. Top. Quantum Electron. **15**, 1646 (2009).
[41] J. Watrous, *The Theory of Quantum Information* (Cambridge University Press, Cambridge, England, 2018).
[42] L. Marrucci, C. Manzo, and D. Paparo, Optical spin-to-orbital angular momentum conversion in inhomogeneous anisotropic media, Phys. Rev. Lett. **96**, 163905 (2006).
[43] L. Marrucci, E. Karimi, S. Slussarenko, B. Piccirillo, E. Santamato, E. Nagali, and F. Sciarrino, Spin-to-orbital conversion of the angular momentum of light and its classical and quantum applications, J. Opt. **13**, 064001 (2011).
[44] F. Cardano, F. Massa, H. Qassim, E. Karimi, S. Slussarenko, D. Paparo, C. de Lisio, F. Sciarrino, E. Santamato, R. W. Boyd *et al.*, Quantum walks and wavepacket dynamics on a lattice with twisted photons, Sci. Adv. **1**, e1500087 (2015).
[45] F. Cardano, M. Maffei, F. Massa, B. Piccirillo, C. De Lisio, G. De Filippis, V. Cataudella, E. Santamato, and L. Marrucci, Statistical moments of quantum-walk dynamics reveal topological quantum transitions, Nat. Commun. **7**, 11439 (2016).
[46] T. Giordani, L. Innocenti, A. Suprano, E. Polino, M. Paternostro, N. Spagnolo, F. Sciarrino, and A. Ferraro, Entanglement transfer, accumulation and retrieval via quantum-walk-based qubit–qudit dynamics, New J. Phys. **23**, 023012 (2021).
[47] A. Gratsea, M. Lewenstein, and A. Dauphin, Generation of hybrid maximally entangled states in a one-dimensional quantum walk, Quantum Sci. Technol. **5**, 025002 (2020).
[48] X. Wang, Y. Qian, J. Zhang, G. Ma, S. Zhao, R. Liu, H. Li, P. Zhang, H. Gao, F. Huang *et al.*, Learning to recognize misaligned hyperfine orbital angular momentum modes, Photonics Res. **9**, B81 (2021).